

# PCCP

Accepted Manuscript



This is an *Accepted Manuscript*, which has been through the Royal Society of Chemistry peer review process and has been accepted for publication.

*Accepted Manuscripts* are published online shortly after acceptance, before technical editing, formatting and proof reading. Using this free service, authors can make their results available to the community, in citable form, before we publish the edited article. We will replace this *Accepted Manuscript* with the edited and formatted *Advance Article* as soon as it is available.

You can find more information about *Accepted Manuscripts* in the [Information for Authors](#).

Please note that technical editing may introduce minor changes to the text and/or graphics, which may alter content. The journal's standard [Terms & Conditions](#) and the [Ethical guidelines](#) still apply. In no event shall the Royal Society of Chemistry be held responsible for any errors or omissions in this *Accepted Manuscript* or any consequences arising from the use of any information it contains.

# Relaxation Dynamics of Helium Nanodroplets After Photodissociation of a Dopant Homonuclear Diatomic Molecule. The Case of $\text{Cl}_2@(^4\text{He})_N$

Arnau Vilà,<sup>a</sup> Miguel González<sup>a,\*</sup> and Ricardo Mayol<sup>b,\*</sup>

<sup>a</sup> Departament Química Física i IQTC, Universitat de Barcelona, c/ Martí i Franquès, 1, 08028 Barcelona, Spain.

<sup>b</sup> Departament d'Estructura i Constituents de la Matèria, Universitat de Barcelona, c/ Martí i Franquès, 1, 08028 Barcelona, Spain.

## Abstract

To investigate the quantum dynamics of the relaxation process of excited helium nanodroplets,  $^4\text{He}_N$ , arising from the photodissociation of  $\text{Cl}_2$  embedded molecules ( $\text{B} \leftarrow \text{X}$  electronic transition), here we have performed a time dependent density functional theory (TDDFT) study considering nanodroplets of different sizes ( $N=50, 100, 200, 300$  and  $500$ ), extending a previous study which was centered on the photodissociation step. The relaxation process takes place in the timescale of several hundred picoseconds and a simple dependence of this process on time has been found. The results have been satisfactorily analyzed in terms of a phenomenological model proposed here and also by applying the Rice-Ramsperger-Kassel (RRK) statistical chemical kinetic model for unimolecular reactions. From what we know, this is the first time that the dynamics of these de-excitation

processes has been studied, opening up a window for understanding them. We expect that this work will encourage further research on this little known but interesting phenomenon.

**Keywords:** helium nanodroplet, helium relaxation, helium vaporization, impurity, homonuclear diatomic, Cl<sub>2</sub>, photodissociation, dynamics, theory, time dependent density functional theory

**Tables:** 2    **Figures:** 7    **Schemes:** 1

**Supporting Information included**

\* Corresponding authors: E-mail: [miguel.gonzalez@ub.edu](mailto:miguel.gonzalez@ub.edu); Fax: +34 93 4021231;

[ricardo.mayol@ub.edu](mailto:ricardo.mayol@ub.edu); Fax: +34 93 4037063

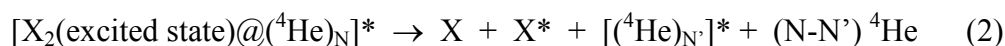
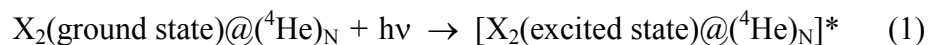
## 1. Introduction

The nanometric length-scale of superfluid helium nanodroplets ( $T = 0.37$  K),  ${}^4\text{He}_N$ , makes these systems very interesting because they are in the midpoint between small molecular clusters and bulk liquid and so, they help in elucidating the properties of quantum fluids and how they emerge due to the increasing of the system size. The use of doping impurities inside  ${}^4\text{He}_N$  allows considering two types of studies. Thus, sometimes they are used as a probe, in order to obtain a better understanding of the droplet system, while in other cases the interest is focused in the impurity itself and the helium nanodroplets are the matrix where the study of the properties of these chemical species is performed. This last kind of studies includes, e.g., spectroscopy<sup>1</sup> and chemical synthesis of different products, ranging from small metastable molecules up to metallic clusters such as nanoparticles<sup>2</sup> and nanowires.<sup>3</sup>

From a theoretical standpoint many efforts have been made during the last two decades involving the study of the structure, energetics and spectroscopy of doped  ${}^4\text{He}_N$ .<sup>4</sup> Moreover, the study of the real-time dynamics of processes occurring in (atomic) doped helium nanodroplets has become an intensive area of research during the last few years.<sup>5</sup> Nowadays, the theoretical study of these processes is mainly carried out within the time dependent density functional theory (TDDFT) framework; and from these investigations exciting properties of  ${}^4\text{He}_N$  have been revealed, such as, e.g., the existence of the critical Landau velocity in helium nanodroplets.<sup>6</sup> Moreover, it should also be noted the possibility of using the ZPAD (zero point augmented dynamics) theoretical approach<sup>7,8</sup> for studying the dynamics of processes involving helium nanodroplets and atoms or molecules, although up to now this method has only been applied to small nanodroplets ( $N=100$ ).<sup>7</sup>

Recently, we presented a theoretical approach to describe the photodissociation quantum dynamics of homonuclear molecules embedded in superfluid 4-helium nanodroplets.<sup>9</sup> It corresponds to a hybrid quantum mechanical time-dependent method that combines TDDFT (helium density) and wavefunction (diatomic molecule wavepacket) dynamics. Despite the relative simplicity of this type of processes, the investigation pointed out the presence of remarkable features of the reaction dynamics in this quantum solvent.

The problem under consideration here can be interpreted as a chemical reaction taking place in a system with a large number of atoms and involving three steps:



where the  $(N-N')$   $^4\text{He}$  and  $(N'-N'')$   $^4\text{He}$  terms only denote the total number of vaporized  $^4\text{He}$  atoms in the photodissociation of the  $X_2$  diatomic molecule and relaxation of the nanodroplet, respectively (maximum  $N = 500$ ); see also Scheme 1. Moreover, the symbol “\*” indicates that the corresponding species are in an excited state (electronic excited state in the case of  $X_2$  and one of the  $X$  atoms and, simply, distorted geometry in the case of the nanodroplet).

The excitation and photodissociation processes (steps (1) and (2)) have been considered by us in a previous contribution<sup>9</sup> and, in order to complete the investigation of the whole process (i.e., steps (1)-(3)), here we present the study of the final step. This corresponds to the nanodroplet relaxation which takes place once the  $X$  and  $X^*$

photofragments have left the droplet. To do this, we have employed the same quantum dynamics theoretical approach (TDDFT) as in ref. 9 and, as far as we know, this is the first time that the dynamics of this type of relaxation process has been examined.

As it will be seen this process is mediated by the evaporation of helium atoms. The evaporative process of liquid helium has been investigated in the literature but from two different perspectives: quantum evaporation<sup>10</sup> and evaporative cooling.<sup>11,12</sup> The former aims to examine the escape of a helium atom from the liquid surface due to the scattering with the quasiparticles excitations of liquid helium (phonons and rotons).

The evaporative cooling process that takes place when the droplets have been just formed (from the aggregation of many atoms) and decrease their energy and temperature until they reach the thermodynamic equilibrium, via the evaporation of a significant number of helium atoms, has been investigated using statistical treatments.<sup>11,12</sup> The present work is somewhat related to the evaporative cooling, though the origin and degree of excitation energy and number of helium atoms of the droplets examined are quite different.

The paper is organized as follows: Section 2 presents a brief description of the theoretical methods employed; Section 3 reports the main results obtained and the corresponding analysis and interpretation of results and, finally, the summary and conclusions are given in Section 4.

## 2. Theoretical methods

The description of the superfluid liquid 4-helium adopted in this study is based on a TDDFT approach, using the phenomenological Orsay-Trento functional,<sup>13</sup> where, as usual<sup>5,6,9,14,15</sup> and consistently with the study of the previous photodissociation process (eq (2)),<sup>9</sup> for computational reasons (see below) we have neglected in the functional the non-local contributions to the correlation energy and the backflow term. A detailed description of this procedure can be found in our previous contribution on the  $X_2@(^4\text{He})_N$  photodissociation process<sup>9</sup> and here we just give a brief explanation.

It should be noted that only recently it has been possible to carry out theoretical studies on the dynamics of chemical and physical processes involving superfluid helium nanodroplets and atoms or molecules.<sup>5,6,9,14,15</sup> These studies have used the approximations of the Orsay-Trento functional indicated above, due to the major complications of numeric type arising from the consideration of the non-local contribution to the correlation energy and backflow terms. Moreover, when it has been possible to compare the theoretical results achieved using these approaches with the experimental data a quite satisfactory agreement has been found.<sup>5,6,15</sup>

Furthermore, here we have performed several checks in order to obtain a deeper insight on the influence of these two terms on the relaxation dynamics. We have only considered the nanodroplet with  $N=50$  as these calculations are very costly. Inclusion of the non-local contribution to the correlation energy term in the functional leads to results that are very close (nearly identical) to the ones obtained from the approach used in the present work, while the inclusion of the previous term and the backflow term also leads to results

which are very close to the present results. However, the propagation of the equations of motion when the backflow term is involved is very unstable for numerical reasons (imaginary contribution to  $\frac{\delta \mathcal{E}_c[\rho_{He}]}{\delta \rho_{He}}$  (see eq 4)); and in this situation we have been able to obtain satisfactory propagations only for small time intervals of about 5 ps. Anyway, these checks allowed us to verify the validity of the approximation used in this work which, as indicated before, corresponds to the present state-of-the-art to describe theoretically the dynamics of processes involving superfluid helium nanodroplets, as indicated before.

Within the TDDFT framework, the equation of motion is obtained by minimizing the quantum action, varying the complex effective wave function of helium, which is defined by  $|\Psi_{He}(\mathbf{R}_{He}, t)|^2 \equiv \rho_{He}(\mathbf{R}_{He}, t)$ , where  $\rho_{He}(\mathbf{R}_{He}, t)$  is the helium density at the time  $t$  for the nanodroplet  $(x, y, z)$  point specified by the position vector  $\mathbf{R}_{He}$ . This treatment leads to the following non-linear Schrödinger-like equation:

$$i\hbar \frac{\partial}{\partial t} \Psi_{He}(\mathbf{R}_{He}) = \left[ -\frac{\hbar^2}{2m_{He}} \nabla^2 + \frac{\delta \mathcal{E}_c[\rho_{He}]}{\delta \rho_{He}} \right] \Psi_{He}(\mathbf{R}_{He}) \quad (4)$$

This equation has been solved discretizing the space in a Cartesian coordinate grid of points, whose size has been optimized for each droplet ( $N = 50, 100, 200, 300$  and  $500$ ). The grid spacing used is the same employed for describing the photodissociation process,<sup>9</sup> i.e.,  $0.09 \text{ \AA}$  for the  $z$ -axis (Cl-Cl molecular axis) and  $0.35 \text{ \AA}$  for the  $x$  and  $y$  axes.

The numerical integration of eq 4 has been carried out by means of a fourth order Adams predictor-corrector-modificator method,<sup>16</sup> initiated by a fourth order Runge-Kutta method,<sup>17</sup> using a time step of  $0.35 \text{ fs}$  ( $23.3$  times larger than the time step used in the

photodissociation process),<sup>9</sup> while the evaluation of the derivatives for the kinetic energy terms has been performed in momentum space (Fourier transform using the FFTW package<sup>18</sup>). Furthermore, in order to avoid non-physical reflections of the effective wave function of helium in the limits of the grid, quartic negative imaginary potentials (NIPs)<sup>19</sup> have been applied in these regions. More details on the theoretical methods used can be found in ref. 9.

### 3. Results and discussion

As already indicated above (cf. eqs 1-3 and Scheme 1), there are two steps strongly related to the photodissociation process of Cl<sub>2</sub> embedded in helium nanodroplets. Even though the separation of steps 2 and 3 is useful for the intuitive understanding of the global process (photodissociation of the diatomic molecule and relaxation of the nanodroplet), they are really not so clearly separated, and this point should be clarified in order to define the beginning of the process of interest in this work.

From a purely energetic point of view, we could consider that the relaxation process begins when the first helium atom evaporates from the nanodroplet, releasing some energy with it. However, this would lead to widely different initial conditions for the relaxation process, depending on the initial size of the droplet. This is because after a very short time from the Cl<sub>2</sub>(X<sup>1</sup>Σ<sub>g</sub><sup>+</sup>) + hν → Cl<sub>2</sub>(B<sup>3</sup>Π<sub>u</sub>(0<sub>u</sub><sup>+</sup>)) electronic transition, energy is being transferred from the molecule to the helium and shortly after the helium evaporation begins. With this criterion there would be initial conditions of the systems for which the impurities would be still inside the droplet (big droplet sizes), while in other cases the resulting atomic

photofragments would be about to leave the helium environment (small droplet sizes).

Taking into account this fact, we have considered that the relaxation process begins when the chlorine atoms have left the droplet and are far enough, so that there is practically no interaction between the droplet and them. This corresponds to the situation in which the formation of the reaction products of the second step, eq (2), has occurred. According to this choice, in computational terms we have defined the starting point of the relaxation process as the time for which the norm of the diatomic wavepacket in the system is less than  $\approx 5.0 \cdot 10^{-5}$ . This approximately corresponds to a ratio between the helium-Cl<sub>2</sub> interaction energy and the helium energy (sum of the kinetic, potential and correlation energies of helium, i.e., the helium-Cl<sub>2</sub> interaction energy is not included) of less than or equal to 1 part in 1000.

Although this choice of the initial time for the relaxation process is reasonable, of course it is not the only available option. Thus, e.g., another possibility would be to consider the time at which the two chlorine dissociating atoms leave the interior of the nanodroplet (or, alternatively, to consider an intermediate choice between this option and the one used in the present work). If the specific choice is kept under reasonable terms it should not be critical, because it should lead to an analogous behavior as that reported here. Moreover, it should be noted the slowness of the relaxation process (see below), which corresponds to a time scale that is about two orders of magnitude higher than the variability that arises when defining the zero time of this process.

Useful data to show that the initial time considered is a reasonable choice is provided in the last three figures reported in the SI. The time evolution of the energy of the

nanodroplet per  $^4\text{He}$  atom considering as initial time the excitation of  $\text{Cl}_2$  from the ground (X) to the excited (B) state is shown in Figure S6. Moreover, it can be seen that the trends observed for two especially interesting initial times for the nanodroplet relaxation (the photodissociation time and the formation of products (cf. eq 2)) are similar (Figures S7 and S8), although, of course, the initial excitation energy is larger in the former case. Here it is important to remember that in this work we are focusing our attention into the relaxation dynamics of the nanodroplet once the Cl atoms are located outside the nanodroplet, and for initial time choices intermediate between the two times indicated above we can expect similar tendencies.

From the results obtained it can be seen that the more excited nanodroplets at the beginning of the relaxation process are the smaller ones, even though they have received less energy from  $\text{Cl}_2$ .<sup>9</sup> The values of several relevant properties at the relaxation initial time definition are reported in Table 1, and from now on to label each nanodroplet we have kept its initial number of  $^4\text{He}$  atoms (i.e.; the number before the  $\text{Cl}_2$  electronic transition;  $N_0 = 50, 100, 200, 300$  and  $500$ ).

The main properties (extensive variables) obtained in the TDDFT calculations showing the temporal evolution of the helium nanodroplets relaxation are the energy ( $E$ ) and the number of  $^4\text{He}$  atoms ( $N$ ). In Figure 1 is shown how  $E$  and  $N$  evolve with time and it can be seen that the main energy and  $^4\text{He}$  atoms release takes place during the first  $\approx 5$  ps. Using these plots an estimation of the time scale of the relaxation process can be inferred, taking into account the asymptotic character of the two variables with time. The time-scale obtained is of the order of several hundred of picoseconds, and the concrete values of the relaxation times are somewhat dependent on the nanodroplets considered. Some additional

useful information is provided in Figure S1 ( $E$  vs  $t$ ; 0-10 ps) and Figure S2 (% of  $^4\text{He}$  atoms in the nanodroplets vs time; 0-150 ps) of SI.

However,  $E$  and  $N$  are extensive physical properties and due to this they are not the most suitable properties to follow the relaxation process. In order to achieve a better characterization of the relaxation process, the intensive magnitude “energy per  $^4\text{He}$  atom” ( $e \equiv E/N$ ) has been considered for all the excited nanodroplets (cf. Figure 2) and compared to the ground state corresponding values ( $e_{gs}$ ). This has been done by calculating a wide set of pure helium nanodroplets in the ground state (ranging from 25 to 10000  $^4\text{He}$  atoms), using the same DFT functional approximation employed in the TDDFT study and fitting the  $e_{gs}$  values to the well-known liquid drop model,<sup>20</sup>

$$e_{gs}(N) \equiv \frac{E_{gs}(N)}{N} = a_v + a_s N^{-\frac{1}{3}} + a_c N^{-\frac{2}{3}} + a_d N^{-1} \quad (5)$$

, where  $a_v$ ,  $a_s$ ,  $a_c$ , and  $a_d$  correspond to the volume energy, surface energy, curvature energy, and correction parameters, respectively ( $a_v = -7.156$  K,  $a_s = 17.47$  K,  $a_c = 4.027$  K and  $a_d = -26.33$  K, while  $a_d N^{-1}$  is a correction factor which allows to include small droplets in the fitting). In order to better compare the relaxation process for the different droplets, we define the excitation energy per  $^4\text{He}$  atom as  $\Delta e(N, t) \equiv e(N, t) - e_{gs}(N)$ , which is also an intensive property. This property defines the asymptotic limit in which the relaxation process will be fully accomplished, i.e.,  $\lim_{t \rightarrow \text{relax. time}} \Delta e(N, t) = 0$ .

The excitation energy per  $^4\text{He}$  atom decreases when increasing the nanodroplet size (Figure 3 and Figures S3 and S4 in SI). As already mentioned, this occurs because the main

energy exchange taking place between the  $\text{Cl}_2$  molecule and the droplet is produced when the chlorine atoms collide with the first solvation shell (which is common for all the droplets), and the time needed to complete the photodissociation process increases with the size. Hence, big nanodroplets have more time to release energy, even though energy exchange is still present during the translational motion of the Cl atoms inside the droplet.

The excitation energy per  $^4\text{He}$  atom decreases with time and the de-excitation or relaxation curves,  $\Delta e$  vs.  $t$ , fit well to a simple inverse law with respect to time (Figure S4 in SI). Two dynamic regimes are evident, the high and low excitation energy per  $^4\text{He}$  atom regions, linked by a transition zone. Furthermore, the related  $1/\Delta e$  vs  $t$  dependence is plotted in Figure 3 and Figure S3 in SI and it is observed that also in this case all curves follow the same pattern. The fits shown in Figure 3 correspond to the low excitation regime and it comes out that the slopes of the straight lines increase with the droplet size until they reach an, essentially, limit value for the biggest droplets considered here (i.e.,  $N_0 = 200, 300$  and  $500$ ). These facts suggest that for this regime the dissipation energy time evolution depends on the size but with a threshold or reference value from which this dependency almost disappears. A somewhat similar though more complex behavior is found for the high excitation region (cf. Figure S3 in SI).

Regarding the dynamics of the relaxation mechanism of the nanodroplets, the analysis of the time evolution of the helium density (Figure 4) shows that it is common to all of them. This is consistent with the similarity we have also found for other properties of the nanodroplets.

Thus, at the beginning of the relaxation process intense oscillations are evident in the helium density, that are particularly important along the z axis (axis along which the photodissociation of the Cl<sub>2</sub> molecule has previously occurred), specially at low times. The magnitude of the oscillations gradually decreases with time, becoming essentially coincident first the helium densities along the x and y axis (which were already rather similar at the beginning of the relaxation). Besides, the helium density along the z axis, the most initially disturbed density, is becoming progressively more similar to the density along the x and y axis and, finally, all the densities become essentially coincident.

In Figure 4 the radial density of helium (i.e., the density along the z axis) and the density in the xy and xz planes are presented, for the relaxing helium nanodroplet with  $N_0=500$  and considering small ( $t=3.0$  ps) and large ( $t=518.7$  ps) relaxation times. Analogous plots but for  $N_0=100$  have been reported in Figure S5 of the SI. Moreover, in Movies 1-3 ( $N_0=100$ ) and Movies 4-6 ( $N_0=500$ ) of the SI the time evolution of these densities are shown, taking into consideration time intervals that correspond to low, intermediate and high relaxation times.

To obtain a deeper insight into the relaxation process, we propose a very simple model where we have assumed that the change of energy per <sup>4</sup>He atom of the nanodroplet per evaporated <sup>4</sup>He atom  $\left(\frac{de}{dN}\right)$  is proportional to the intensive excitation  $\Delta e$ ; i.e., we consider that this is the only driving force governing the amount of energy carried by an evaporated <sup>4</sup>He atom. Of course, this may be considered as a rough approximation, since we neglect both the size and shape effects, but the slight dependency observed for the shape of the de-excitation vs. time evolution curves with the nanodroplet size supports the main idea of this model. From this approach we expect to be able to account for all the

nanodroplets studied, regardless of their size, since this would show the characteristics of the common part of all the droplets, i.e., the liquid helium.

From the calculation of the  $\frac{de}{dN}$  derivative and the representation of these data versus the  $\Delta e$  excitation per  $^4\text{He}$  atom (Figure 5), it follows that the  $\frac{de}{dN}$  vs  $\Delta e$  plots almost follow a straight line for the low excitation regime, which points out the common nature of all of them (i.e., the superfluid liquid helium). This trend does not occur for the high excitation regime, where a more complex dependency of  $\frac{de}{dN}$  is evident. Therefore, although the simple model proposed here does not account for all the physics of the relaxation process, we infer that the excitation energy per  $^4\text{He}$  atom of the nanodroplet is the main driving force that dictates the de-excitation energy per  $^4\text{He}$  atom of the nanodroplet resulting from the evaporation of one helium atom.

We have also explored the suitability of describing the relaxation kinetics as a unimolecular fragmentation process, i.e., as a unimolecular chemical reaction of a very large molecule (the whole nanodroplet). In this context, we have fitted the obtained TDDFT data to the well known Rice-Ramsperger-Kassel (RRK) statistical kinetics model for unimolecular reactions.<sup>21</sup>

In short, this model describes the molecular internal degrees of freedom as a set of coupled harmonic oscillators, and the molecular fragmentation is supposed to occur when a certain amount of energy is placed in one of them. Thus, for a given excess energy of the system,  $\mathcal{E}$  (see below), the fragmentation rate constant,  $k(\mathcal{E})$ , is determined by calculating the probability to have an energy above a threshold value,  $\mathcal{E}_0$ , in a given oscillator (i.e., in

the bond to be broken). The parameters of the model are the number of oscillators,  $s$ , the characteristic harmonic vibrational frequency of the oscillators,  $\nu$ , and the threshold energy  $\mathcal{E}_0$  required for the fragmentation (evaporation of a helium atom in the present case), and the classical RRK rate constant has the following expression:<sup>21</sup>

$$k(\mathcal{E}) = \nu \left(1 - \frac{\mathcal{E}_0}{\mathcal{E}}\right)^{s-1} \quad (6)$$

The rate constant  $k(\mathcal{E})$  has been evaluated for each single atom vaporization process that happens during the relaxation process of each selected nanodroplet (Figure 6). Besides, since we have employed a continuous theoretical method (TDDFT) to describe the nanodroplets dynamics, in order to apply the RRK model we have performed a numerical integration to obtain the mean values of the properties ( $k$ ,  $\mathcal{E}$ ) associated to each atomic evaporation.

For each nanodroplet, we have fixed the  $\mathcal{E}_0$  value to the average binding energy per <sup>4</sup>He atom of the set of ground state nanodroplets ranging from  $N=N_i$  to  $N=N_f$ , i.e.,

$$\mathcal{E}_0 = \frac{1}{(N_f - N_i)} \int_{N_i}^{N_f} e_{gs}(N) N dN, \quad (7)$$

where the subscripts  $f$  and  $i$  stands for final and initial number of helium atoms of the relaxing nanodroplet, respectively. It has been checked that variations in the  $\mathcal{E}_0$  value do not lead to significant changes in the profiles of the curves in Figure 6, but only to small variations in the  $\nu$  parameter (in the fitting procedure to obtain the optimal  $\nu$  and  $s$

parameters of eq 6). Following the same idea, the  $\mathcal{E}$  value of this model has been calculated as the mean value of the excitation energy obtained for each atomic evaporation (where the “i” subscript in the following equation refers to an arbitrary single atom vaporization and not to the initial situation of the system):

$$\mathcal{E} = \int_{N_i}^{N_i-1} (E(N, t) - Ne_{gs}(N)) dN \quad (8)$$

The obtained points for the rate constants (TDDFT calculations) and the RRK fitting parameters ( $\nu$ ,  $s$ ) are collected in Figure 6 and Table 2, respectively. The agreement between the quantum dynamics TDDFT results and this fitting is quite good for all the nanodroplets studied and the determined values of the RRK parameters are reasonable.

Finally, we have also investigated a large number of average intensive properties in order to determine possible correlations between them. We have found rather clear correlations in two cases: in the percentage of  $^4\text{He}$  atoms evaporated in the relaxation process and in the increment of the mean energy per  $^4\text{He}$  atom in the nanodroplet corresponding to the evaporation of one  $^4\text{He}$  atom, i.e.,  $\frac{e_f - e_i}{N_f - N_i}$ . More concretely, it has been found that these properties follow a linear dependence with respect to the initial excitation energy per  $^4\text{He}$  atom of the nanodroplets (Figure 7). This also reinforces our assumption that  $\Delta e$  is the most important property guiding the relaxation process.

The number of evaporated  $^4\text{He}$  atoms ranges from 10 ( $N_0=50$ ) to 19 ( $N_0=500$ ), and in Figure 7 is shown that the percentage of  $^4\text{He}$  atoms evaporated during the relaxation

process depends in a significant way on the nanodroplet size: 23.0, 15.1, 9.4, 7.3, and 3.9% for  $N_0=50, 100, 200, 300,$  and  $500,$  respectively (where, the percentages are given with respect to the corresponding  $N_i$  values; cf. Table 1). This results from the fact that the smaller the nanodroplet size the higher the excited character of the nanodroplet at the initial relaxation time, as indicated at the beginning of this section.

#### 4. Summary and conclusions

The relaxation dynamics of superfluid helium nanodroplets,  ${}^4\text{He}_N$  ( $N=50, 100, 200, 300$  and  $500$ ) that takes place after the photodissociation of a  $\text{Cl}_2$  embedded molecule [arising from the  $\text{Cl}_2(X^1\Sigma_g^+) + h\nu \rightarrow \text{Cl}_2(B^3\Pi_u(0_u^+))$  electronic transition] has been studied at the time-dependent DFT theoretical level, extending a previous investigation of our group which was focused on the photodissociation process. To the best of our knowledge, this is the first time that the dynamics of these de-excitations has been investigated, opening up a window for understanding them.

The relaxation mechanism is common for all nanodroplets and it occurs in the timescale of several hundred picoseconds. Moreover, a simple dependence ( $\Delta e$  vs  $t$  inverse law) has been found for the evolution of the excitation energy per  ${}^4\text{He}$  atom of the nanodroplet with time. This applies to the two dynamic regimes (the high and low excitation energy per  ${}^4\text{He}$  atom regions) even though a somewhat more complex behavior is evident for the former case.

The results have been rationalized by means of two simple models. The first one consists in a phenomenological approach, where it is proposed that the energy released by

evaporation of a  $^4\text{He}$  atom is, simply, proportional to the excitation energy per  $^4\text{He}$  atom of the nanodroplet. Despite its simplicity, the accuracy for this model is accurate enough for low excitation energies and points out the common aspects of the different nanodroplets, since the parameters of the fit are unique for all of them. The second model corresponds to the well-known RRK statistical kinetic model for unimolecular reactions, from which a quite satisfactory agreement has been also obtained.

We hope that this study will encourage further research on this little-known and interesting research topic involving superfluid nanodroplets of helium-4.

### Acknowledgements

This work has been supported by the Spanish Ministry of Science and Innovation (projects refs. CTQ2011-27857-C02-01 and FIS2011-28617-C02-01), and we also want to acknowledge the support from the Autonomous Government of Catalonia (A. V. predoctoral fellowship and projects refs. 2009SGR 17, 2014SGR 25 and XRQTC).

**Electronic supplementary information (ESI) available:** (a) **Figures:** time evolution of the energy of the nanodroplets, 0-10 ps (Figure S1); time evolution of the percentage of  $^4\text{He}$  atoms in the nanodroplets, 0-150 ps (Figure S2); time evolution of the inverse of the excitation energy per  $^4\text{He}$  atom for the nanodroplets in the high excitation regime (Figure

S3); time evolution of the excitation energy per  $^4\text{He}$  atom in the nanodroplets (Figure S4); helium density for the relaxing nanodroplet with  $N_0=100$  at two selected times (Figure S5); time evolution of the energy per  $^4\text{He}$  atom in the nanodroplets after the  $\text{B} \leftarrow \text{X}$  excitation of  $\text{Cl}_2$  (Figure S6); time evolution of the energy per  $^4\text{He}$  atom in the nanodroplets for two different initial times (Figure S7); time evolution of the inverse of the excitation energy per  $^4\text{He}$  atom in the nanodroplets for two different initial times (Figure S8); **(b) Movies:** time evolution of the helium density for the relaxing nanodroplet with  $N_0=100$  at low, intermediate and high time intervals (movies 1-3, respectively); the same as before for  $N_0=500$  (movies 4-6, respectively). See DOI:...

**Tables:****Table 1.** Values of some properties at the relaxation initial time.

$N_0$	50	100	200	300	500
Elapsed time from B←X transition (ps)	3.65	3.36	3.43	4.30	7.08
Cl <sub>2</sub> wave packet norm	$5.0 \cdot 10^{-5}$	$4.6 \cdot 10^{-5}$	$5.0 \cdot 10^{-5}$	$4.9 \cdot 10^{-5}$	$4.1 \cdot 10^{-5}$
$N_i^a$	43.48	91.78	190.22	287.89	480.96
Interaction energy (K) <sup>b</sup>	$4.9 \cdot 10^{-4}$	$6.2 \cdot 10^{-2}$	$6.0 \cdot 10^{-2}$	$8.6 \cdot 10^{-2}$	$7.7 \cdot 10^{-2}$
Helium energy (K)	179.01	150.08	-60.33	-565.69	-1844.47
$e$ (K) <sup>c</sup>	4.12	1.64	-0.32	-1.96	-3.84
Interaction energy/Helium energy (‰)	$2.7 \cdot 10^{-6}$ (0.00)	$4.1 \cdot 10^{-4}$ (0.41)	$-9.9 \cdot 10^{-4}$ (- 0.99)	$-1.5 \cdot 10^{-4}$ (- 0.15)	$-4.2 \cdot 10^{-5}$ (- 0.04)

<sup>a</sup> Initial number of He atoms.

<sup>b</sup> Cl<sub>2</sub>-helium interaction energy.

<sup>c</sup> Energy per <sup>4</sup>He atom.

**Table 2.** Optimal parameters for the RRK statistical model.

$N_0$	<b>50</b>	<b>100</b>	<b>200</b>	<b>300</b>	<b>500</b>
$\nu$ (ps <sup>-1</sup> )	1.09	2.32	3.18	4.41	5.95
$s^{-1}$	31.8	50.7	64.0	70.7	104.1
$\epsilon_0$ (K)	2.33	3.28	4.09	4.48	4.90

**Figure and scheme captions:**

**Figure 1.** Time evolution of the energy (up) and number of  $^4\text{He}$  atoms (down) for nanodroplets of different sizes.

**Figure 2.** Time evolution of the energy per  $^4\text{He}$  atom for different nanodroplets.

**Figure 3.** Time evolution of the inverse of the excitation energy per  $^4\text{He}$  atom for different nanodroplets.

**Figure 4.** Helium density (radial (i.e., along the z axis), xy plane and xz plane densities) for the relaxing helium nanodroplet with  $N_0=500$  at  $t=3.0$  ps (left) and  $t=518.7$  ps (right).

**Figure 5.** Derivative of the energy per  $^4\text{He}$  atom with respect to the number of helium atoms versus the excitation energy per  $^4\text{He}$  atom, for different nanodroplets.

**Figure 6.** Rate constant for  $^4\text{He}$  atoms evaporation versus the excitation mean energy for different nanodroplets. The curves correspond to the fitting according to the RRK rate constant expression (eq 6; see text).

**Figure 7.** Percentage of  $^4\text{He}$  atoms evaporated (up) and ratio between the change in the energy per  $^4\text{He}$  atom in the nanodroplet and the number of  $^4\text{He}$  atoms evaporated (down) for the relaxation processes investigated, and in both cases as a function of the initial excitation energy per  $^4\text{He}$  atom.

**Scheme 1.** Graphic representation of the three steps involved in the investigation of the photodissociation of embedded  $\text{X}_2$  diatomic molecules in helium nanodroplets and associated processes: (a) electronic excitation of  $\text{X}_2$ ; (b) photodissociation of  $\text{X}_2$ ; (c) relaxation of the nanodroplet. In (b) and (c) some  $^4\text{He}$  atoms of the nanodroplet are vaporized.

Figures:

Figure 1 (up)

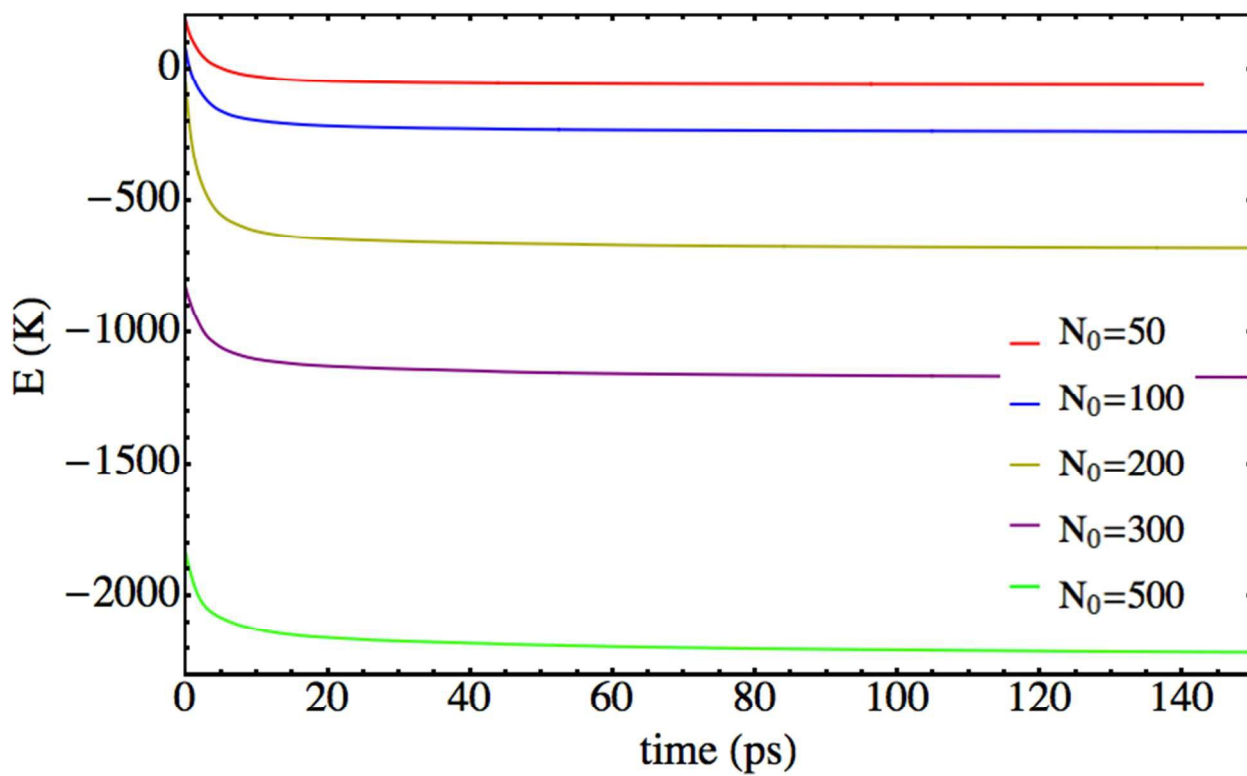


Figure 1 (down)

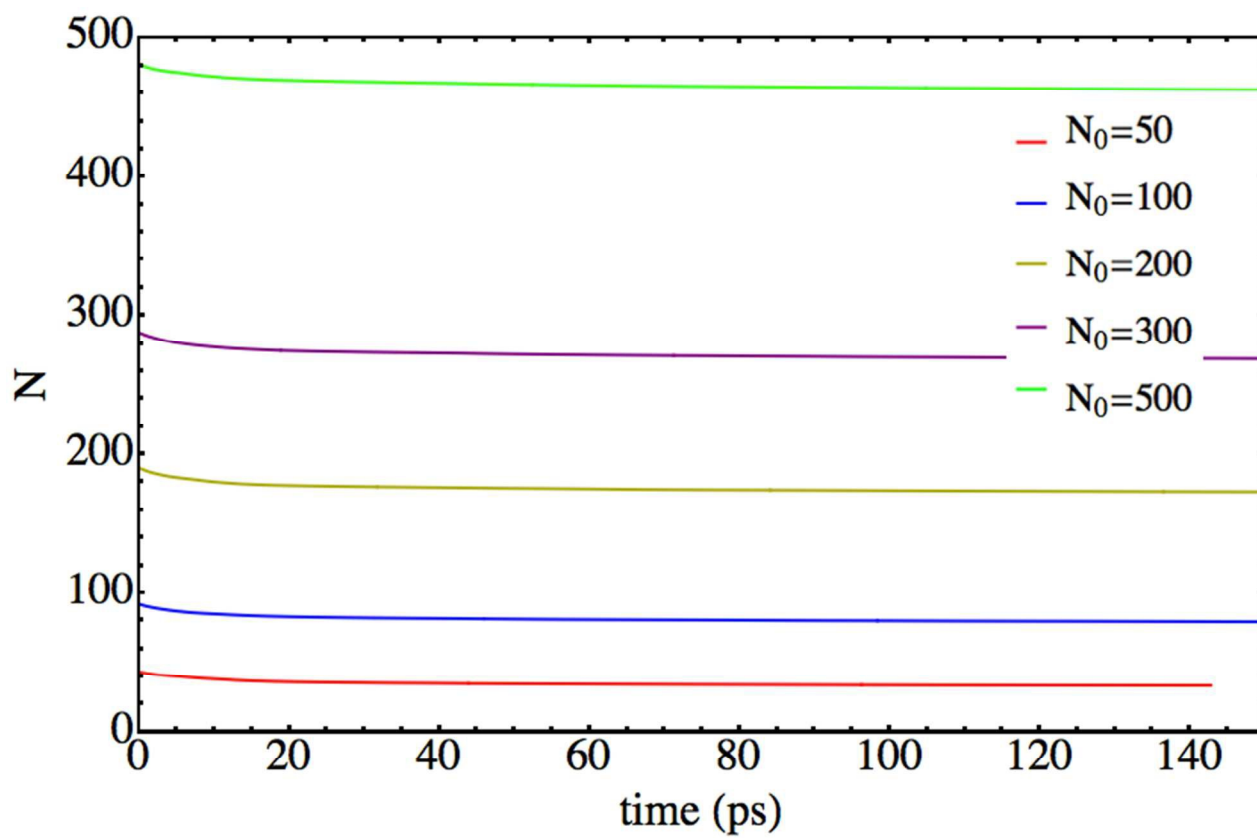


Figure 2

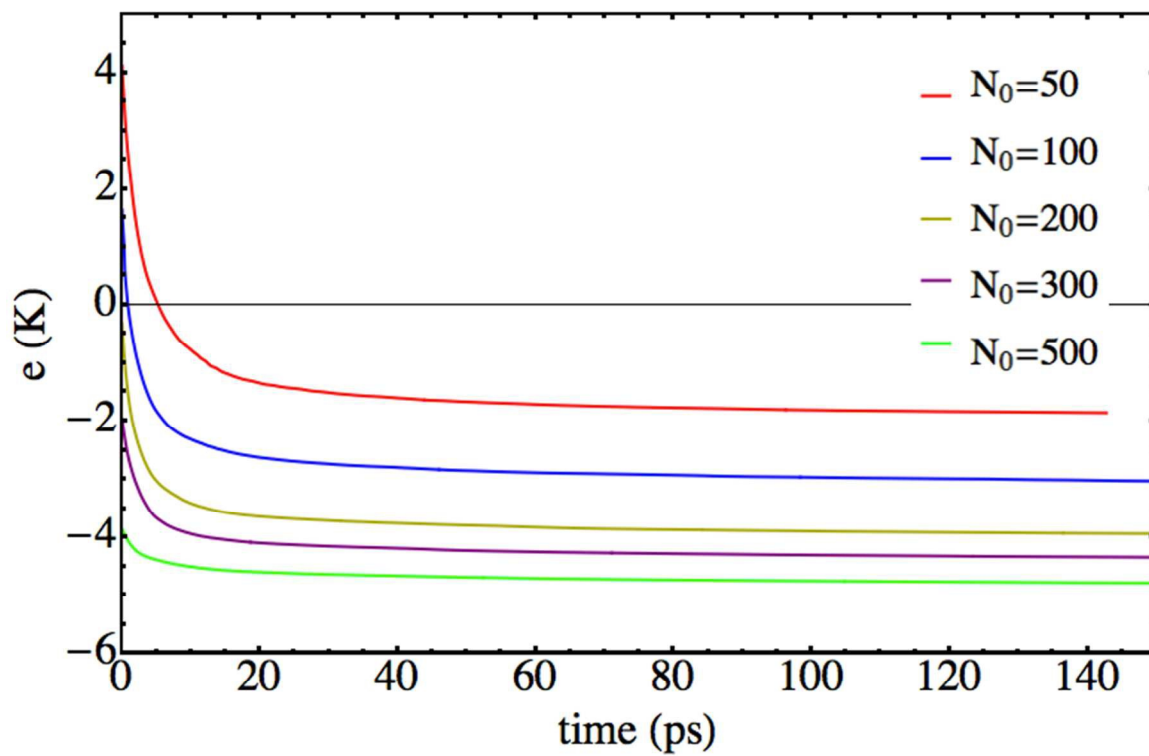


Figure 3

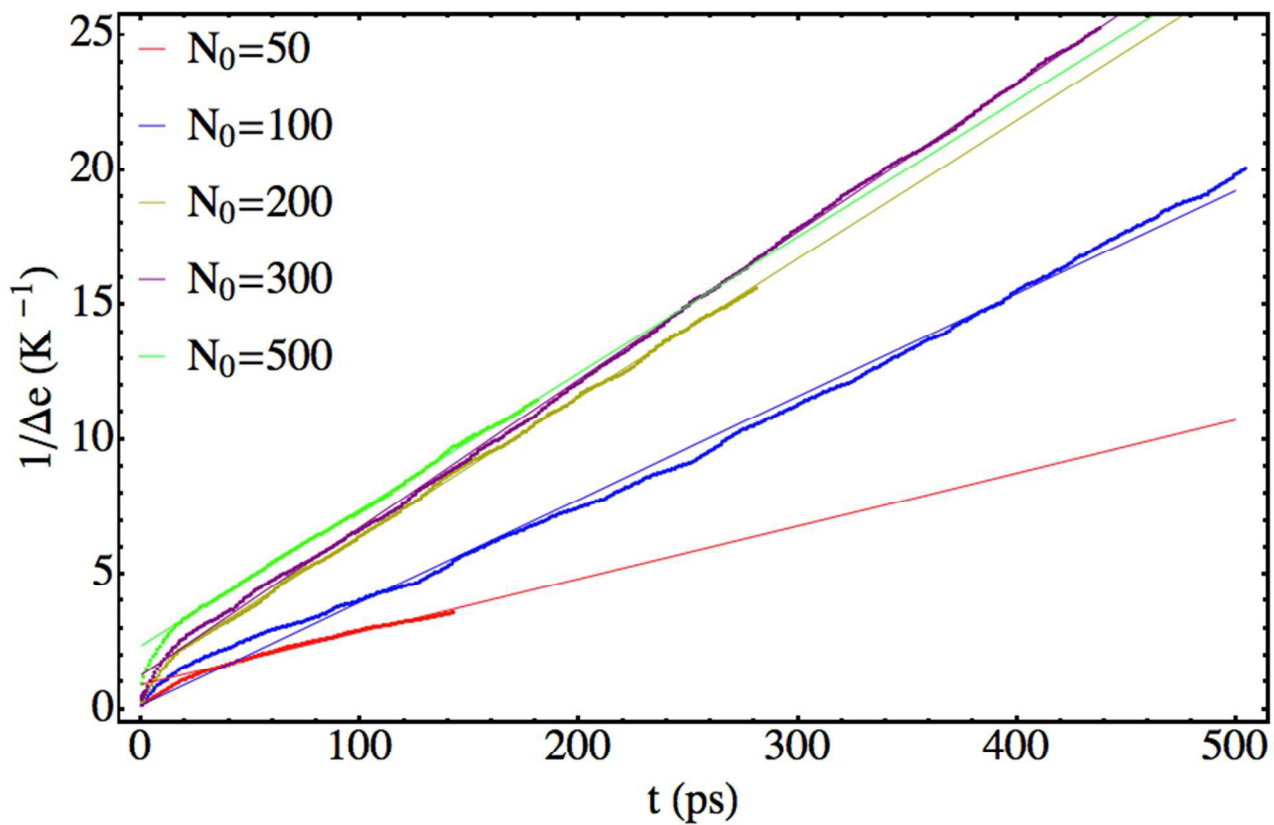


Figure 4

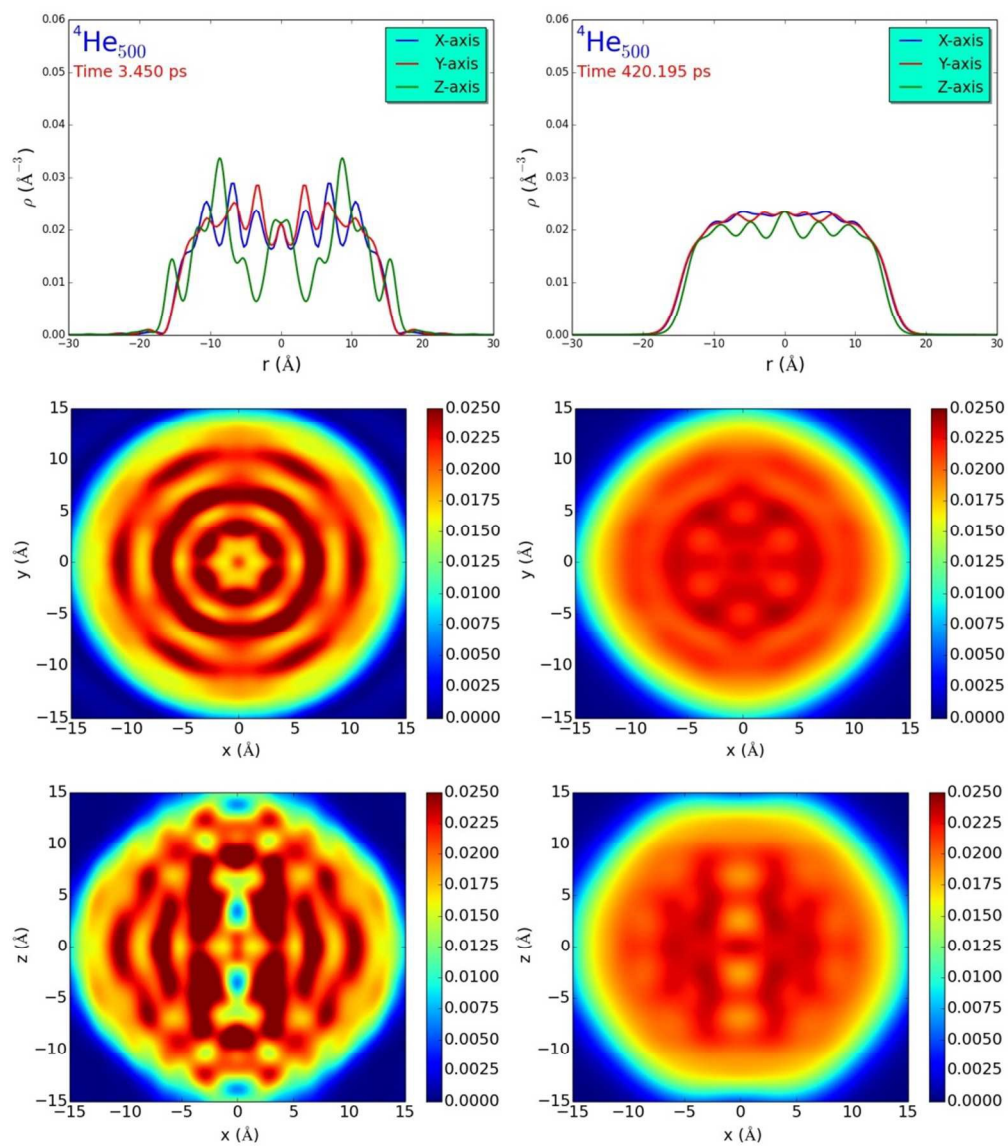


Figure 5

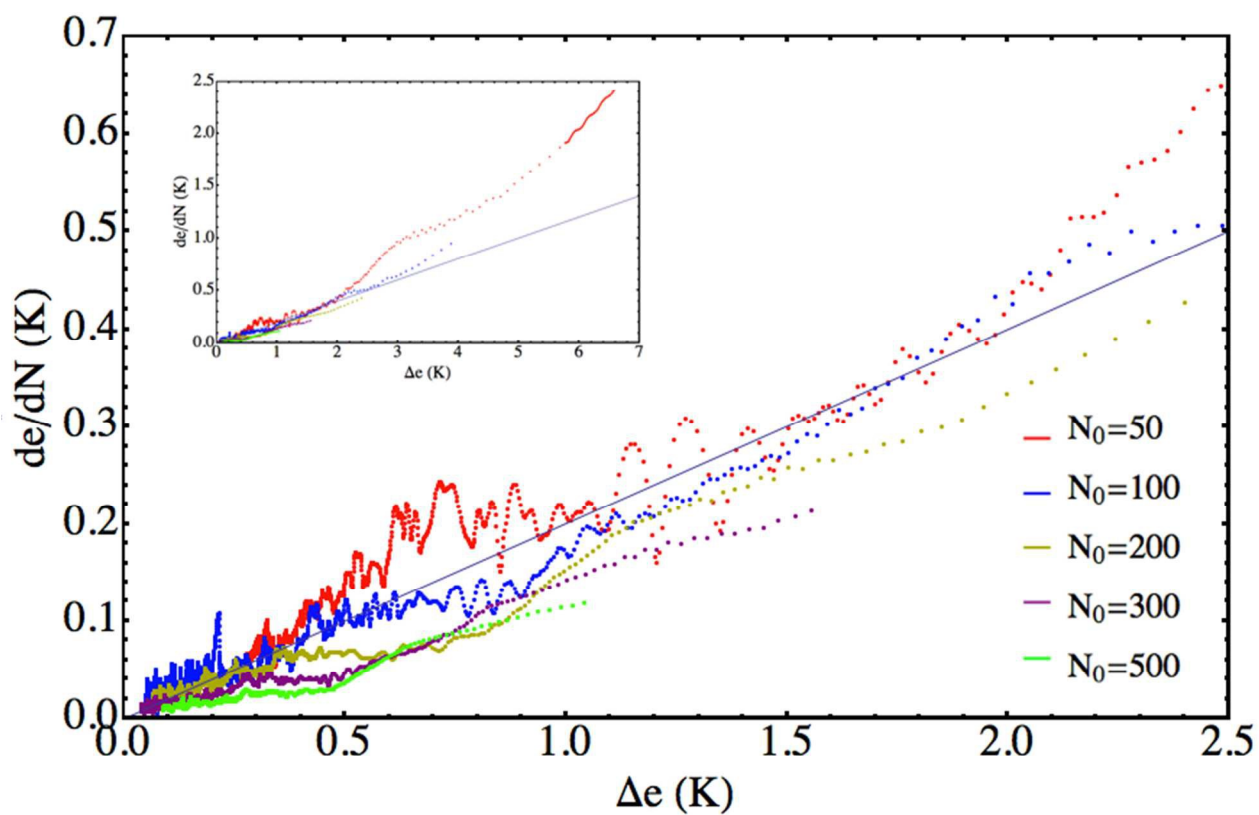


Figure 6

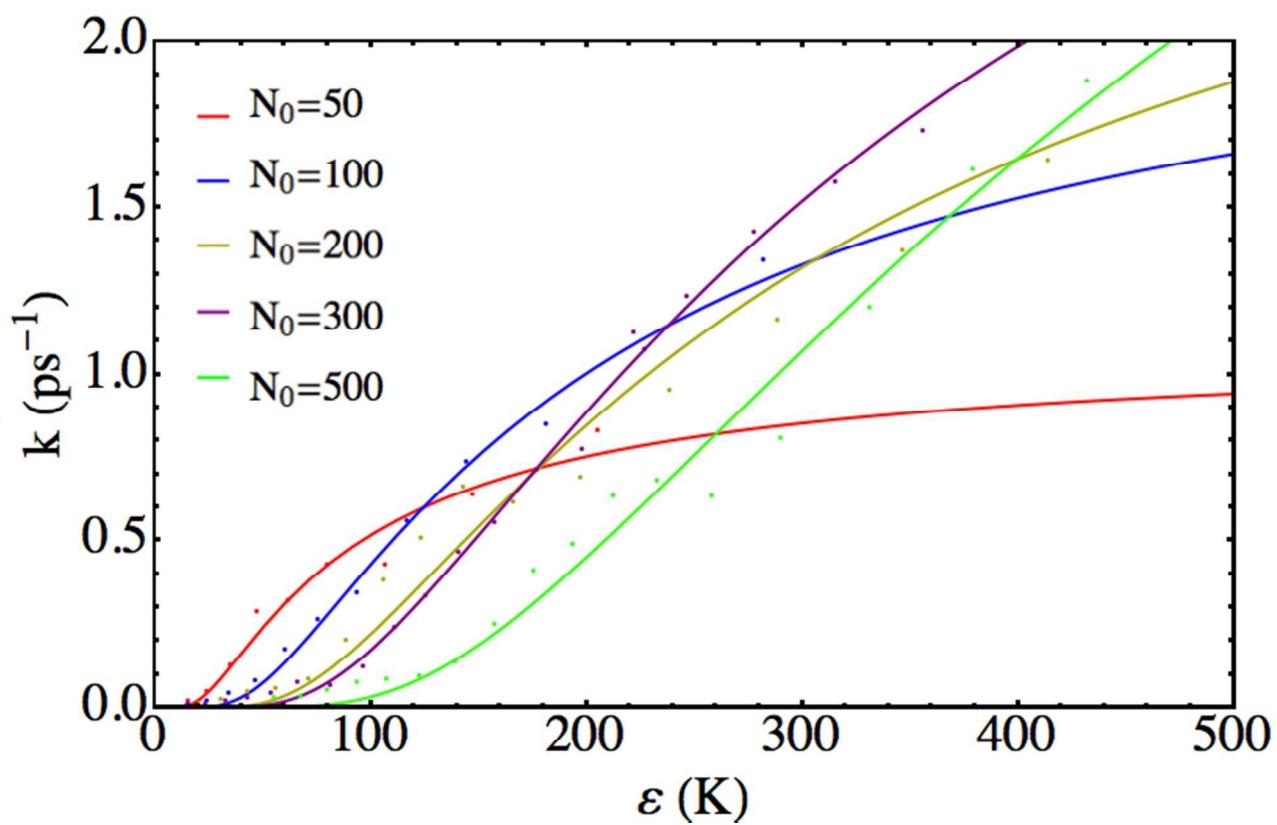


Figure 7 (up)

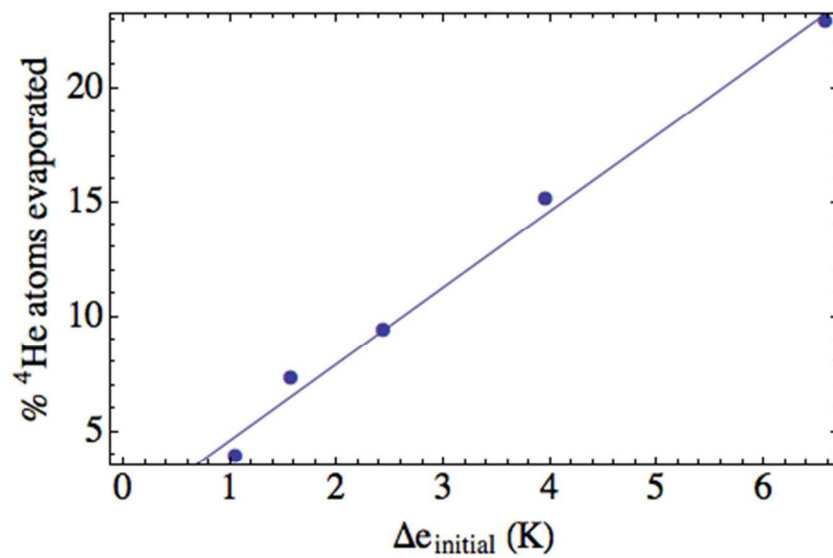
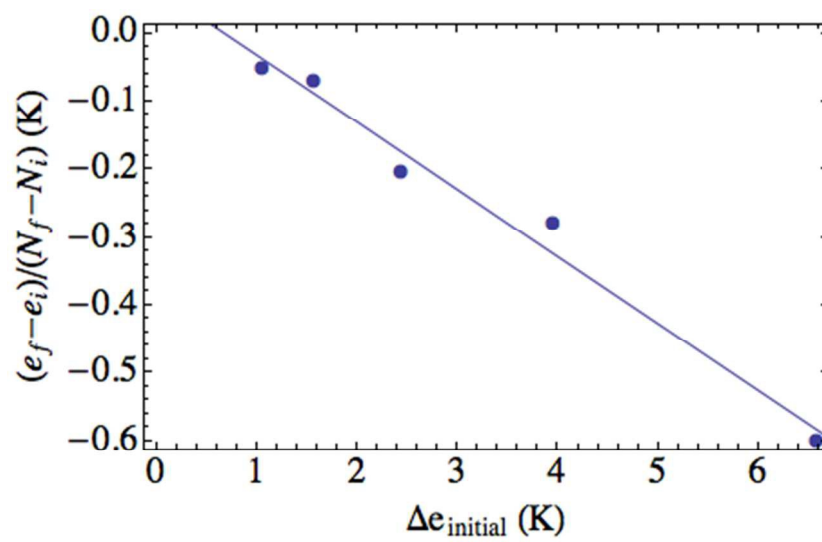
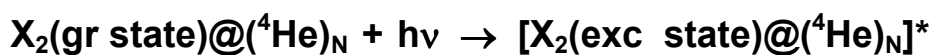


Figure 7 (down)



## Scheme 1

**1. X<sub>2</sub> electronic transition****2. X<sub>2</sub> photodissociation****3. <sup>4</sup>He nanodroplet relaxation**

## References

---

- (1) J. P. Toennies and A. Vilesov, *Angew. Chem. Int. Ed.*, 2004, **43**, 2622.
- (2) S. Yang, A. M. Ellis, D. Spence, C. Feng, A. Boatwright, E. Latimer and C. Binns, *Nanoscale*, 2013, **5**, 11545.
- (3) E. Latimer, D. Spence, C. Feng, A. Boatwright, A. M. Ellis and S. Yang, *Nano Lett.*, 2014, **14**, 2902.
- (4) M. Barranco, R. Guardiola, S. Hernández, R. Mayol, J. Navarro and M. Pi, *J. Low Temp. Phys.*, 2006, **142**, 112.
- (5) D. Mateo, A. Hernando, M. Barranco, E. Loginov, M. Drabbels and M. Pi, *Phys. Chem. Chem. Phys.*, 2013, **15**, 18388.
- (6) N. B. Brauer, S. Smolarek, E. Loginov, D. Mateo, A. Hernando, M. Pi, M. Barranco, W. J. Bruma and M. Drabbels, *Phys. Rev. Lett.*, 2013, **111**, 153002.
- (7) D. Bonhommeau, M. Lewerenz and N. Halberstadt, *J. Chem. Phys.*, 2008, **128**, 054302.
- (8) U.-T. Wesley, N. Halberstadt, C. Meier and M. Mella, *J. Chem. Phys.*, 2012, **137**, 014304.
- (9) A. Vilà, M. González and R. Mayol, *J. Chem. Theory Comput.*, 2015, **11**, 899.
- (10) F. Dalfovo, M. Guilleumas, A. Lastri, L. Pitaevskii and S. Stringari, *J. Phys.: Condens. Matter*, 1997, **9**, L369.

- 
- (11) D. M. Brink and S. Stringari, *Z. Phys. D*, 1990, **15**, 257.
- (12) K. K. Lehmann and A. M. Dokter, *Phys. Rev. Lett.*, 2004, **92**, 173401.
- (13) F. Dalfovo, L. Pricauptenko, S. Stringari and J. Treiner, *Phys. Rev. B*, 1995, **52**, 1193.
- (14) A. Leal, D. Mateo, A. Hernando, M. Pi and M. Barranco, *Phys. Chem. Chem. Phys.*, 2014, **16**, 23206.
- (15) D. Mateo, F. Gonzalez and J. Eloranta, *J. Phys. Chem. A*, 2015, **119**, 2262.
- (16) A. Ralston, in *Mathematical Methods for Digital Computers*, eds. A. Ralston and H. S. Wilf, John Wiley & Sons, New York, 1960, vol. 1, pp. 95-109.
- (17) R. J. Thompson, *Commun. ACM*, 1970, **13**, 739.
- (18) M. Frigo, and S. G. Johnson, *IEE Proceedings*, 2005, **93**, 216.
- (19) A. Vibók and G. G. Balint-Kurti, *J. Phys. Chem.* 1992, **96**, 8712.
- (20) A. Bohr and B. Mottelson, *Nuclear Structure*, Benjamin, New York, 1975, vol. 2.
- (21) J. I. Steinfeld, J. S. Francisco and W. L. Hase, *Chemical Kinetics and Dynamics*, Prentice Hall, Englewood Cliffs, 1998.